Automated Patient-Specific C1-C2 Posterior Cervical Fusion Screw Trajectory Planning using 3D Deep Learning

Yau-Zen Chang[1,2], Sanny Kumar Sahani[1] and Chieh-Tsai Wu[2]

[1]Chang Gung University, Taiwan
[2]Linkou Chang Gung Memorial Hospital, Taiwan

2024 International Joint Conference on Neural Networks (IJCNN) | 979-8-3503-5931-2/24/$31.00 ©2024 IEEE | DOI: 10.1109/IJCNN60899.2024.10651187

***Abstract*—Posterior cervical fusion at C1-C2 is technically challenging due to the complex anatomy of this region. Optimal screw trajectory planning is crucial, yet currently relies extensively on imaging and manual adjustment. This work investigates an automated planning approach using 3D deep learning and immersive visualization for intuitive verification and editing. Vertebral CTs were converted to 3D point clouds, and ideal screw entry/exit locations were annotated by experienced technicians and approved by neurosurgeons. These ideal locations were replaced with 60-point clusters, with cluster size optimized to balance segmentation and recovery accuracy. Two deep networks were developed based on the PointNet architecture to efficiently learn both local and global 3D vertebral shape features of C1 and C2, respectively. Augmentation techniques generated 11,000 unique training datasets from 50 qualified patient CTs. Cluster center points identified the closest vertebral surface points as suggested entry/exit locations. Performance was quantified by deviation from ideal paths and proximity to vertebral surfaces. Testing on 10 cases not involved in training showed trajectories within 2.7 mm of surgeon-validated ground truth. A preliminary Microsoft HoloLens 2 interface demonstrates the potential of intuitive 3D validation and modification. Overall, deep learning segmentation of vertebral point clouds successfully generated automated, patient-specific screw plans for challenging C1-C2 fixation, eliminating manual measurement errors. The immersive interface further aids preoperative planning. This work demonstrates the potential of deep-learning technologies to enhance precision and safety in posterior cervical fusion.**

Keywords—deep neural networks, 3D point cloud segmentation, posterior cervical fusion, screw path planning, mixed reality.

I. INTRODUCTION

Posterior cervical fusion techniques to stabilize the delicate C1-C2 spinal levels have posed significant surgical challenges historically due to the complex anatomy and technical constraints [1-3]. While modern methods like the Harms technique [4] provide biomechanical stability, ensuring precise and safe screw placement at the C1-C2 pedicles requires advanced expertise to account for anatomical variations [5-7]. Furthermore, intraoperative navigation relies heavily on imaging to verify due to limited visibility [5,8]. Few approaches in the literature effectively address the path planning difficulties. Therefore, developing automated, patient-specific solutions for optimal C1-C2 screw trajectory planning remains an open challenge, given cervical anatomy constraints [7,9-11].

This work addresses this gap through an automated screw path planning methodology using 3D deep learning. Our approach leverages the multi-layer perceptrons (MLPs) and the max-pooling for feature learning on 3D point clouds [12,13]. By representing the C1-C2 anatomy as point cloud models from patient CTs, our proposed neural networks can segment the vertebrae and identify optimal screw paths tailored to each patient's anatomy. The networks are trained on expert-labeled entry and exit points to learn the complex relationships between anatomical shapes and ideal screw trajectories.

The proposed 3D point cloud segmentation approach for screw trajectory planning shows strong potential to significantly improve precision, safety, and efficiency in this anatomically and technically demanding C1-C2 fixation procedure.

Moreover, mixed reality technology has the potential to provide an intuitive visualization of screw paths before surgery, allowing for evaluation and editing. In this work, we investigate the basic interface design of this technology.

II. METHODS

Our neural network's semantic segmentation capabilities are utilized in proposing optimal screw paths. First, the vertebral model is converted to a 3D point cloud representation. The network then segments this point cloud, identifying clusters corresponding to the desired entry and exit points. We determine the precise entry and exit locations by finding the surface points closest to each cluster's geometric center. Connecting the entry and exit points defines the final screw path, as shown in Fig. 1. This automated pipeline enables screw path identification directly from the vertebral anatomy without extensive manual measurement, planning, or imaging guidance.

A. Preparation of training data

The C1-2 vertebrae models used in this work were derived from CT scans. These models were converted into 3D point clouds using the Open3D library (version 0.17) [14], as shown in Fig. 2. Point clouds provide detailed spatial representations by encoding the coordinates (x, y, z) for each point. The density of points, determined by the scanning resolution, is important for accurate segmentation and classification. For each training dataset, 3,000 points were uniformly sampled

from the original 3D model containing approximately 32,000 points.

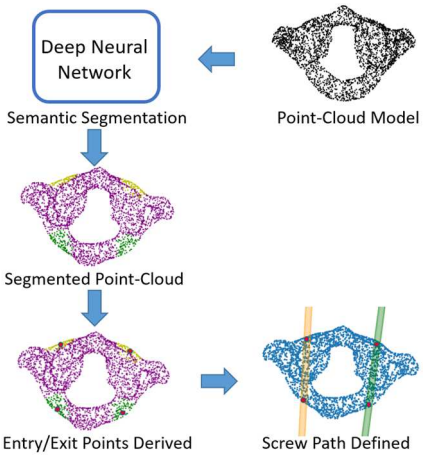

Fig. 1. Overview of the proposed deep learning approach for automatic screw path identification on C1 and C2 vertebral models. Entry and exit points are derived from semantic segmentation and used to define screw trajectories.

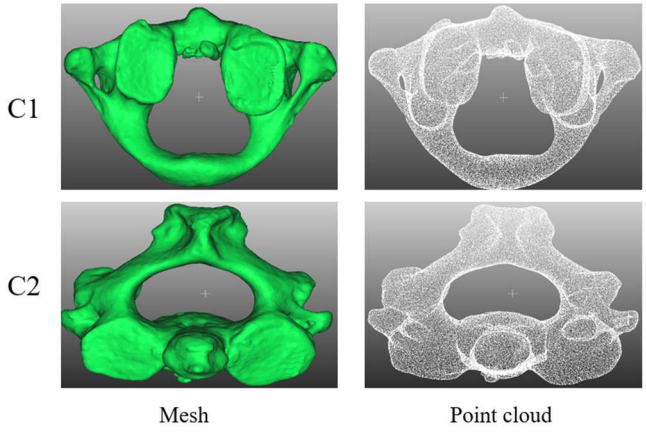

Fig. 2. Point-cloud data were generated from mesh data using Open3D 0.17 [14].

To generate training targets for our supervised learning models, technicians first identified the ideal entry and exit screw locations on the 3D models of C1 and C2 vertebrae. Surgeons then validated these locations. We transformed the identified entry and exit points as clusters within the vertebral models, effectively framing the location identification task as a 3D semantic segmentation problem.

Specifically, we identified the surface points closest to the ideal locations and designated those as sub-cloud clusters, as shown in Fig. 3. The C1 model with ideal entry and exit points is displayed in Fig. 2a (left), along with the 4 derived sub-cloud clusters corresponding to those locations (Fig. 3a, right). Fig. 3b shows a similar example for C2. Since the vertebral models contained only surface points, we ultimately predicted the entry and exit locations by identifying the closest surface points to each cluster's center. Framing the problem as semantic segmentation in this way allowed us to generate feasible training targets for the supervised learning models.

Our dataset originally consisted of only 50 paired sets of C1 and C2 vertebral models collected from Chang Gung Memorial Hospital. Of these, 10 sets were reserved for model verification. The remaining 40 training sets were insufficient to adequately train a supervised learning model. To augment the limited data, we applied techniques like flipping, resizing, rotating, and translating to the 40 original training sets. This data augmentation generated the additional training examples needed. In total, after augmentation, we obtained 11,520 sets of input vertebral models and corresponding target entry/exit points for model training. We randomly selected 9,126 point-cloud datasets for training and 2,304 for validation.

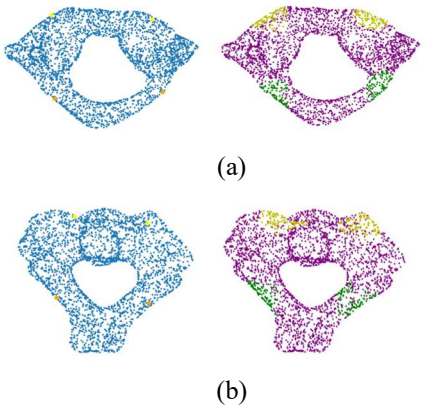

Fig. 3. Generation of training data with labeled sub-clouds from ideal entry and exit points. (a) Left: A C1 point cloud model with ideal entry (orange) and exit (yellow) points. Right: The ideal points are replaced by clustered regions - entry (green) and exit (yellow) sub-clouds. (b) A C2 point cloud model with ideal entry and exit points converted to clustered sub-clouds.

B. Development of deep learning networks for 3D point-cloud segmentation

The deep learning network developed for 3D point cloud segmentation is based on the PointNet architecture [12]. The network processes both local and global features. It uses an input transformation mechanism to maintain point attributes, max pooling to represent high-level features, and joint alignment for accurate segmentation and feature alignment.

As shown in Fig. 4, the architecture begins with a T-net module to ensure label preservation during transformation. T-net predicts affine transformation matrices to align input clouds [12]. This is followed by three feature transformation stages, combining convolution, batch normalization, and ReLU activation. A global max pooling layer then aggregates features across points for permutation invariance.

The network fuses local point attributes and global features. After this, 3 more feature transformation stages process the combined representation. Finally, fully connected layers predict segmentation labels per point. The network effectively segments the point cloud by leveraging local and global contexts.

The model was implemented in TensorFlow 2.6 and trained on NVIDIA RTX 3090 GPUs. We initialized training at a 0.001 learning rate and batch size of 32. Training proceeded for 200 epochs over 12.6 hours. Throughout the training, we monitored the loss and tuned hyperparameters like learning rate and batch size to improve convergence. Through careful configuration, we efficiently trained the network to segment the vertebral models.

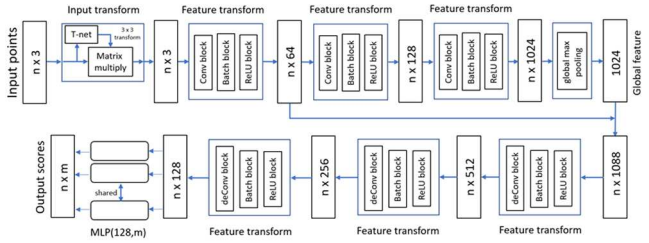

Fig. 4. The proposed deep learning networks for semantic segmentation of 3D point cloud data.

C. *Optimizing cluster point counts for accurate segmentation and path prediction*

The number of points assigned to each cluster during segmentation significantly impacts overall performance. After testing different cluster sizes, we found 60 points per cluster optimally segments the vertebral 3D point-cloud models while enabling accurate screw path recovery. As Fig. 5 shows, a 60-point cluster size achieves the highest concordance between the ideal screw paths (green) and predicted paths (red). Performance declines with too few points, as the clusters cannot segment correctly on the curved vertebral surfaces. Excess points also reduce accuracy by spreading over those curved surfaces. We, therefore, selected 60 points as the ideal cluster size to maximize segmentation and prediction accuracy.

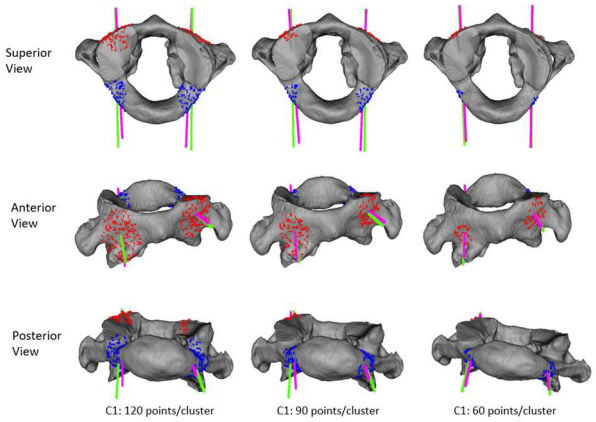

(a)

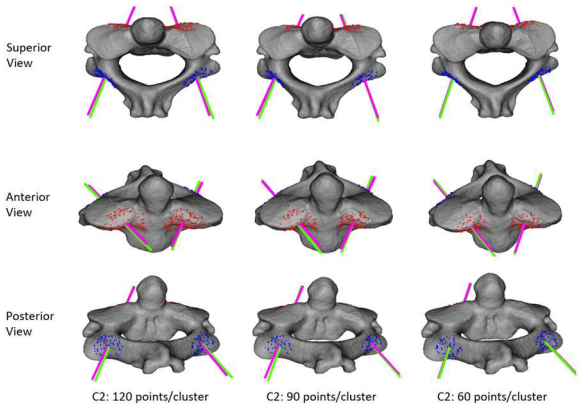

(b)

Fig. 5. Effects of cluster point count on recovered screw path accuracy. Ideal screw paths labeled by technicians are shown in green. Predicted screw paths derived from clustering and segmentation are shown in red. The C1 vertebrae is shown in (a) and the C2 vertebrae is shown in (b). A cluster size of 60 points produced the best path prediction.

D. *Development of a mixed reality interface for screw-path evaluation and editing*

To intuitively visualize, evaluate, and edit the screw paths before surgery, we developed an interface using Microsoft HoloLens 2. The Microsoft HoloLens 2 can render the OBJ models and overlay the planned trajectories for inspection. This allows the surgeon to validate positioning and spacing to ensure safety. While preliminary, this system demonstrates the potential of mixed reality for surgical planning.

Each vertebral model contains approximately 3,000 vertices making up its triangular mesh surface. Using the predicted entry and exit points, we generate screw paths visualized as green (entry) and blue (destination) spheres. These act as handles for easily manipulating the trajectories in 3D space, as demonstrated in Fig. 6.

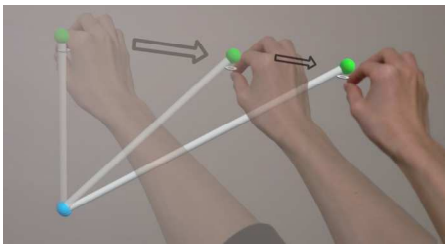

Fig. 6. Manipulating the entry point of a Trajectory Start Site using the mixed reality interface.

To enable path evaluation, we calculate real-time intersections between the trajectory and vertebral surface, determining potential collision triangles. Path/triangle intersections are computed via Barycentric coordinates, as illustrated in Fig. 7(a). Distances from the screw to the surface are also calculated. Surfaces within 1.5 mm of the screw radius turn red, warning of unsafe proximity, as shown in Fig. 7(b).

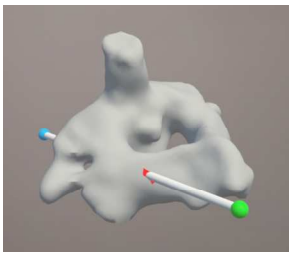

(a)

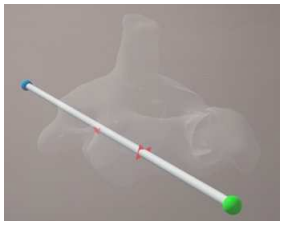

(b)

Fig. 7. Examining the predicted screw trajectory in the HoloLens mixed reality interface. (a) The path is rendered intersecting the vertebral surface, with the entry and exit points shown as spheres. (b) Switching the model to transparent mode improves the visibility of the path. Surfaces within 1.5mm of the screw turn red to indicate unsafe proximity.

Additionally, we implemented movable cut planes to inspect trajectory positions within the vertebral anatomy, as shown in Fig. 8. This cross-sectional view further aids the assessment of the predicted screw placement.

Overall, the Microsoft HoloLens 2 interface provides an intuitive and interactive method for surgeons to validate automated screw planning results before entering the operating room.

Fig. 8. Cross-sectional cut plane enabling inspection of the screw trajectory position within the C2 vertebral anatomy.

III. Results

To validate the performance of our proposed deep learning approach for automated screw path planning, we tested it on 10 reserved vertebral models not used for network training. Example predicted screw paths are visualized in Fig. 9.

We quantitatively evaluated the predicted paths using three key metrics:

- Path deviation - Distance from predicted points to ideal screw path, denoted as *d*.
- Point deviation - Distance between predicted and ideal entry/exit points, denoted as *e*.
- Surface proximity - Distance from the predicted path to the vertebral surface, denoted as *h*.

In summary, d measures how well the overall path matches ground truth, e measures the accuracy of entry/exit points, and h indicates predicted path safety.

Table I through Table III lists the results for the 10 test cases. We also statistically summarize the path quality metrics in Fig. 11. Across all samples, our approach achieved low deviation from ideal entry/exit points and screw paths defined by experienced technicians and validated by neurosurgeons. The predicted paths maintain safe distances from the vertebral surfaces, all more than 1.04 mm. These quantitative results demonstrate our method's efficacy for precise, automated screw trajectory planning directly from vertebral anatomy.

A crucial aspect of our evaluation involved using the Gertzbein Score [15], a well-established grading system for assessing pedicle screw placement accuracy and safety. This validated scale ranges from Grade 0 to Grade 3 based on the degree of screw breach beyond the pedicle cortical boundaries:

Grade 0 indicates optimal placement, with the entire screw residing within the pedicle cortex. This is considered the safest outcome.

Grade 1 reflects a minor breach less than 2 mm outside the pedicle. This carries low to moderate risk.

Grade 2 indicates a breach of 2-4 mm, suggesting higher risk.

Grade 3 denotes a severe breach greater than 4 mm and is the highest-risk outcome.

By applying this standardized methodology, we could objectively evaluate the safety and precision of our algorithm's screw placements. Experienced surgeons assessed our predicted trajectories and assigned a Gertzbein score of Grade 0, confirming their optimal placement completely within the pedicle cortex. Obtaining direct feedback and scoring from neurosurgeons has been invaluable for refining our approach. The excellent Gertzbein grades underscore the practicality of our method and demonstrate its potential to improve surgical planning and execution.

IV. Discussion and Conclusion

Our quantitative evaluation revealed that while the predicted screw trajectories maintained safe distances from critical anatomical structures in most cases, 8 out of 20 test cases resulted in unavoidable cortical breaches. Despite these breaches, the planned paths were still deemed clinically safe by neurosurgical experts, as the minor penetrations were necessitated by unique anatomical constraints, as exemplified in Fig. 10.

In patients with such abnormal vertebral anatomy, alternate stabilization techniques such as lateral mass or pars screws may need to be considered. Our mixed reality-based visualization interface using Microsoft HoloLens 2 will allow surgeons to inspect the automatically planned paths and manually adjust or override them as deemed appropriate. This critical human oversight step will serve as a validation mechanism to ensure surgical safety is not compromised before proceeding with screw placement.

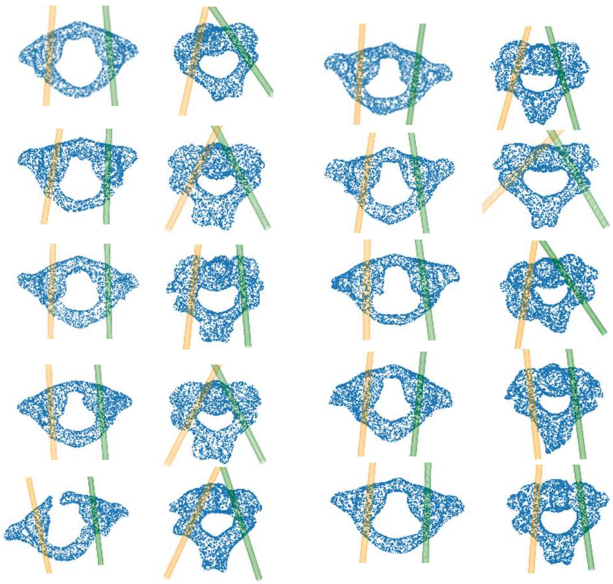

Fig. 9. Predicted pedicle screw paths generated by the deep learning approach on 10 reserved test vertebral models. The left and right screw paths are colored orange and green, respectively.

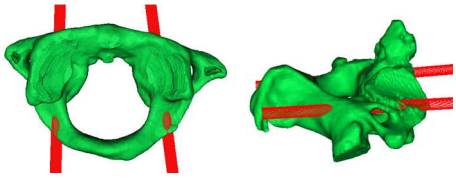

Fig. 10. Unavoidable screw breaches in C1 (left) and C2 (right) due to constrained anatomy. Lateral mass or pars screws may be more optimal in similar cases of limited pedicle dimensions.

In summary, this research represents a pioneering effort in leveraging deep learning for automated preoperative planning of C1/C2 pedicle screw trajectories. We have demonstrated that neural networks can be highly effective at detecting optimal screw entry and exit points tailored to a patient's unique anatomy. When coupled with human surgical expertise for validation, this data-driven approach holds immense potential to enhance precision, reduce errors, and elevate the safety of cervical fixation procedures. Though some anatomical constraints necessitate compromise, our system greatly expedites and optimizes this complex planning process. Moving forward, training the algorithms on larger diverse datasets and advancing to more sophisticated network architectures will further refine the performance. This project sets the stage for transformative innovation at the intersection of spine surgery and artificial intelligence, ultimately aimed at significantly improving clinical outcomes.

TABLE I. THE PATH DEVIATION - DISTANCE FROM PREDICTED POINTS TO IDEAL SCREW PATH.

Patient	Distance to Ideal Path d (mm)			
	Left		Right	
	Entry	Exit	Entry	Exit
1	1.64	1.20	0.85	0.82
2	1.81	1.71	1.97	1.34
3	0.88	0.41	1.62	1.14
4	1.41	1.02	1.24	0.94
5	0.54	0.79	0.63	0.81
6	0.44	0.41	0.62	0.44
7	0.37	0.30	0.57	0.80
8	0.50	0.73	1.35	1.10
9	0.95	0.57	0.34	0.44
10	0.27	0.36	0.31	0.51
Avg.	**0.88**	**0.70**	**0.95**	**0.83**

TABLE II. THE POINT DEVIATION - DISTANCE BETWEEN PREDICTED AND IDEAL ENTRY/EXIT POINTS.

Patient	Deviation between predicted point and ideal point e (mm)			
	Left		Right	
	Entry	Exit	Entry	Exit
1	2.10	1.26	2.14	1.11
2	2.21	1.14	2.35	1.35
3	2.05	1.74	2.32	1.22
4	2.21	1.66	2.25	1.36
5	2.47	1.13	2.35	1.35
6	2.09	0.94	2.32	1.22
7	2.21	1.66	2.25	1.36
8	2.21	1.05	2.35	1.35
9	2.66	1.02	2.32	1.22
10	2.59	1.52	2.55	1.55
Avg.	**2.05**	**1.31**	**2.32**	**1.30**

TABLE III. THE SURFACE PROXIMITY - DISTANCE FROM THE PREDICTED PATH TO THE VERTEBRAL SURFACE.

Shortest distance to the Surface h (mm)		
Patient	**Left**	**Right**
1	1.20	1.89
2	1.25	1.08
3	1.95	1.04
4	1.42	1.35
5	2.36	2.01
6	1.90	1.88
7	1.91	1.93
8	1.95	1.12
9	1.65	1.98
10	1.87	1.95
Avg.	**1.75**	**1.61**

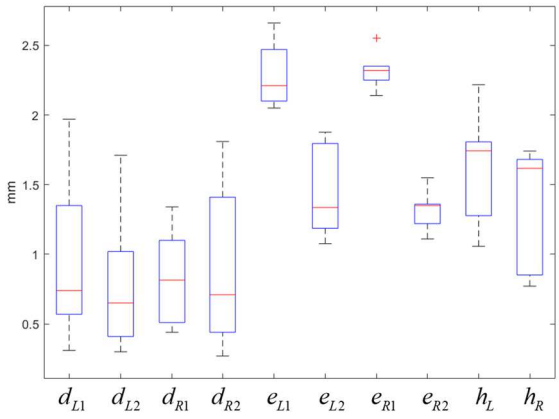

Fig. 11. The box plot summarizing the distributions of the three screw path quality metrics on the test set. In the plot, d measures the deviation from the full ideal screw path trajectory, e measures point deviation from ideal entry/exit locations, and h measures the proximity of the predicted path to the vertebral surface. L/R indicates left and right paths, and 1/2 denotes entry and exit points.

REFERENCES

[1] D.K. Gupta et al., "Development and Validation of Finite Element Analysis Model (FEM) of Craniovertebral Junction: Experimental Biomechanical Cadaveric Study," Spine, 45(16): E978-E988, 2020, doi: 10.1097/BRS.0000000000003491.

[2] C.A. Zárate-Tejero, et al. "Association between Age, Sex and Cervical Spine Sagittal Plane Motion: A Descriptive and Correlational Study in Healthy Volunteers," Life (Basel), 13(2): 461, 2023, doi: 10.3390/life13020461.

[3] J.P.Y. Cheung and K.D.-K. Luk. "Complications of Anterior and Posterior Cervical Spine Surgery," Asian Spine J., 10(2): 385–400, 2016, doi: 10.4184/asj.2016.10.2.385.

[4] M. Sincari, M, "C1-C2 Goel-Harms Fixation, History of the Technique, Free Hand Technique Description," Surg. Sci., 13: 401-409, 2022, doi: 10.4236/ss.2022.139048.

[5] A. Alqurashi, et al., "Accuracy of Pedicle Screw Placement Using Intraoperative CT-Guided Navigation and Conventional Fluoroscopy for Lumbar Spondylosis," Cureus, 13(8):e17431, 2021, doi: 10.7759/cureus.17431.

[6] Y. Zhang, et al., "Improving pedicle screw path planning by vertebral posture estimation," Phys. Med. Biol., 68: 185011, 2023, doi: 10.1088/1361-6560/ace753.

[7] U. Bertram et al., "Man versus machine: Automatic pedicle screw planning using registration-based techniques compared with manual screw planning for thoracolumbar fusion surgeries," Int. J. Med. Robot., 17(6): e2570, 2023, doi: 10.1002/rcs.2570.

[8] Z. Lang, et al., "Posterior atlantoaxial internal fixation using Harms technique assisted by 3D-based navigation robot for treatment of atlantoaxial instability," BMC Surg., 22:378, 2022, doi:10.1186/s12893-022-01826-2.

[9] P.P.M. Sundaram, et al., "Accuracy of Thoracolumbar Pedicle Screw Insertion Based on Routine Use of Intraoperative Imaging and Navigation," Asian Spine J., 15(4):491-497, 2021, doi: 10.31616/asj.2020.0068.

[10] K.D. Baldwin, et al. "Does intraoperative CT navigation increase the accuracy of pedicle screw placement in pediatric spinal deformity surgery? A systematic review and meta-analysis," Spine Deform., 10(1):19-29, 2022, doi: 10.1007/s43390-021-00385-5.

[11] Y.-N. Peng, et al., "Accuracy of robot-assisted versus conventional freehand pedicle screw placement in spine surgery: a systematic review and meta-analysis of randomized controlled trials.," Ann Transl Med., 8(13):824, 2020, doi: 10.21037/atm-20-1106.

[12] C. R. Qi et al., "PointNet: Deep Learning on Point Sets for 3D Classification and Segmentation," In Proc. IEEE Int. Conf. Comput. Vis. Pattern Recognit. (CVPR), Honolulu, HI, USA, 2017, doi: 10.1109/CVPR.2017.16.

[13] C.R. Qi, et al., "PointNet++: Deep Hierarchical Feature Learning on Point Sets in a Metric Space,'' In Proc. Neural Inf. Process. Syst. (NIPS 2017), Long Beach, California, USA, 5105–5114, doi: 10.48550/arXiv.1706.02413.

[14] Qian-Yi Zhou, J. Park and V. Koltun, "Open3D: A Modern Library for 3D Data Processing," arXiv:1801.09847, 2018, doi: 10.48550/arXiv.1801.09847.

[15] J. Neubauer, et al., "Gertzbein and Robbins classification," Radiopaedia.org (Accessed on 24 Jan 2024), doi: 10.53347/rID-82155.